Received: 7 August 2019 | Revised: 29 October 2019 | Accepted: 18 November 2019

DOI: 10.1111/jace.16932

ORIGINAL ARTICLE

Journal of the American Ceramic Society

Hot-pressing platelet alumina to transparency

Andrew P. Schlup | **William J. Costakis Jr.** | **Wolfgang Rheinheimer** | **Rodney W. Trice** | **Jeffrey P. Youngblood**

School of Materials Engineering, Purdue University, West Lafayette, IN, USA

Correspondence
Andrew P. Schlup, School of Materials Engineering, Purdue University, West Lafayette, IN 47907, USA.
Email: aschlup@purdue.edu

Funding information
Army Research Office, Grant/Award Number: W911NF-17-1-0203

Abstract

Alumina powder with a platelet morphology was hot-pressed to transparency with preload pressures of 0-8 MPa, maximum temperatures of 1750-1825°C, maximum pressures of 2.5-80 MPa, and isothermal hold times of 1-7 hours. Optical transmission (in-line and total), as well as optical losses (backward/forward scattering and absorption), of the hot-pressed samples were measured and related to the microstructure. Higher hot-pressing temperatures increase the in-line transmission. A gray discoloration of the samples (indicative of high absorption) was minimized by heat treating the powder in air prior to hot pressing and reducing the preload pressure. Maximum pressures above/below 10 MPa increased porosity, which decreased in-line transmission and increased backward/forward scattering. Lower densities at higher pressures are attributed to a pore-swelling phenomenon. Increasing isothermal hold time decreased porosity, which increased in-line transmission and reduced backward/forward scattering. Best optical properties with an in-line transmission of 65.3% at 645 nm (0.8 mm thick) were achieved by hot-pressing heat-treated platelet alumina powder with a preload pressure of 0 MPa, maximum temperature of 1800°C, maximum pressure of 10 MPa, and an isothermal hold time of 7 hours. This high in-line transmission, despite its large grain size (65 μm), is attributed to crystallographic orientation of the platelets during hot pressing.

KEYWORDS

alumina, hot pressing, materials/properties, optical, platelet-morphology, refractive index, transparent ceramics

1 | INTRODUCTION

Transparent alumina is a candidate for protection applications, such as nose cones, radomes, and ballistic blast shields.[1–3] Alumina can reach optical transparency at high relative densities.[4] However, alumina is birefringent due to its anisotropic rhombohedral crystal structure, causing light scattering at the grain boundaries and limiting transparency.[5] It has been shown that light scattering from birefringence can be minimized by aligning alumina powders along the same crystallographic direction with a high magnetic field prior to densification.[6] While this alignment method is effective, it may be limited in terms of scalability as the high magnetic fields required (>12 T) can only be obtained in small volumes. Therefore, it is important to investigate other methods of alignment. Trice et al[7] found that warm pressing a mixture of thermoplastic polymer and *h*-boron nitride platelets resulted in an aligned microstructure. We propose that this alignment method can be adapted to align high aspect-ratio platelet alumina powders, which could reduce birefringence effects and improve optical properties. However, high relative densities are required to obtain transparency; therefore, the densification behavior of platelet alumina powder must first be understood.

Relative densities greater than 99.95% are required to achieve transparency in polycrystalline ceramics.[8] There are

several different sintering methods used to process alumina to such densities, including pressureless sintering.[5,6,9,10] hot-isostatic pressing (HIP),[8,11–14] spark plasma sintering (SPS),[15–21] and hot pressing.[22,23] Pressureless sintering experiments performed presently with RonaFlair® platelet alumina powder showed that a relative density of approximately 55% could be achieved (1700°C, 1 hour, air). This low density is due to the powder morphology, as the platelets have a diameter of about 11 μm, yielding very low driving forces for sintering. At such low densities, porosity is entirely open porosity, which means that HIP is not available for further densification.[12] Thus, uniaxial pressure as supplied by SPS or hot pressing is required to densify platelet alumina powder. SPS has received much attention for densifying transparent ceramics, including spinel[24–28] and alumina.[15–21] However, for both spinel[25] and alumina,[19] it has been found that lower heating rates (2-10°C/min) resulted in samples with higher transmission. The necessity of lower heating rates defeats the primary benefit of SPS over hot pressing, that is, the ability to heat at rates >100°C/min, which is beneficial for maintaining small grain sizes and decreasing processing time.[29] Graphite hot-press furnaces are a cost-effective alternative, they are capable of heating rates up to 50°C/min, and pressures are only limited by the grade of graphite and die design. These characteristics make hot pressing a promising candidate for densifying platelet alumina powder to transparency.

There is a plethora of research on hot-pressed alumina[30–35] with few investigators reporting attempts to hot-press alumina to transparency. Peelen[4,23] showed that alumina could be sintered to transparency using a continuous hot-pressing method.[36] However, this method requires extremely specialized equipment and precisely machined high-strength alumina dies, a stark contrast to the common graphite dies that are used in conventional hot pressing. Heuer et al[22,37–39] showed that alumina can be hot-pressed to transparency using a method they termed "sinter-forging." Their hot-pressing method used a conventional hot-press furnace and a graphite die, but their method differed from conventional hot pressing in that uniaxial pressure was not applied until the maximum temperature. Heuer et al[37] claimed that by applying the pressure at the maximum temperature, substantial primary recrystallization occurs in the powder compact, which assists in densification. However, they used an equiaxed-morphology alumina powder in their studies,[22,37–39] as have all other studies aiming to produce transparent alumina.[1–6,8–21] To the extent of the author's knowledge, there have been no reported attempts to hot-press platelet-morphology alumina powder to transparency.

Optical losses in transparent polycrystalline alumina occur due to forward scattering, backward scattering, surface reflection, and absorption,[8] and understanding how these optical losses are manifested in a sample are important in determining how to minimize the losses. In transparent alumina, forward and backward scattering are caused by residual porosity due to the significant difference in refractive index between polycrystalline alumina and gas in the pores ($\Delta n = 0.76$).[8] If all porosity is eliminated, polycrystalline alumina can still have forward scattering losses due to grain-boundary reflection and refraction.[8] Grain-boundary reflection is small and can be neglected. However, alumina is inherently birefringent, meaning that the refractive index is anisotropic, resulting in refraction at the grain boundaries that is significant and cannot be ignored.[8] Apetz et al[8] calculated that for an angle of incidence of 45° and the maximum Δn (0.008), light will be deflected a maximum of 0.28° from its original direction, which is further exacerbated across several grain boundaries. Therefore, a fully dense sample with high forward scattering must have a refractive index mismatch at the grain boundaries.

Surface reflection is caused by the difference in refractive index between the polished ceramic surface and air. It is due to either smooth (specular reflection) or rough surfaces (diffuse surface scattering). In the current work, the diffuse surface scattering has been minimized by polishing all samples. Samples had similar surface reflective losses when compared to a polished single-crystal sapphire standard (as described in Section 2). Therefore, losses due to surface reflection have been ignored in this study.

Absorption in transparent ceramics is caused by secondary phases,[8] and qualitatively manifests as a discoloration in a transparent sample. Several of the samples in this study have a distinct gray discoloration, which is a common defect observed in transparent spinel.[40,41] In the case of spinel, the primary mechanisms for absorption were identified to be carbon contamination, oxygen vacancies, and impurities in the raw powder. It is believed that similar mechanisms are responsible for the discoloration in this study. Using the direct absorption measurement technique described in Section 2, the amount of light lost due to secondary phases can be determined.

In this work, we report on the sintering behavior and resulting optical properties of hot-pressed platelet alumina powder with no intentional alignment prior to hot pressing. The effects of hot-pressing parameters on the densification and optical properties of platelet-morphology alumina will be discussed, with an emphasis on the optical losses and how they are manifested in the samples. Parameters include maximum temperature, powder heat treatment, preload pressure, maximum pressure, and isothermal hold time.

2 | EXPERIMENTAL PROCEDURE

2.1 | Powder preparation

RonaFlair® White Sapphire (Merck KGaA, EMD Performance Materials) platelet alumina powder was used. It has a platelet morphology as shown in Figure 1, with a diameter and thickness of approximately 11 and 0.5 μm, respectively. The impurity

content of the powder was measured via inductively coupled plasma mass spectrometry, and was found to contain 0.012% Ca, 0.002% Cr, 0.018% Fe, 0.001% K, 0.26% Na, 0.015% Si, and 0.002% Ti (weight percent). The platelet alumina powder was washed in ethanol and heated at 105°C overnight in air to evaporate the ethanol, then sieved through a 250 μm nylon mesh to break apart soft agglomerates (P1 in Table 1). For some samples, the ethanol-washed/evaporated powder was heated-treated at 1100°C for 1 hour in air prior to sieving (P2 in Table 1). The specific surface area of the ethanol-washed and heat-treated powder was 2.00 ± 0.03 and 1.13 ± 0.02 m^2/g, respectively, as measured by the Brunauer-Emmett-Teller method. The mass-loss of the ethanol-washed and heat-treated powders were measured by high-temperature thermogravimetric analysis (TGA) under flowing air.

2.2 | Hot pressing

Hot pressing was performed using a graphite die with an inner diameter of 25.4 mm. Molybdenum foil sheets (0.14 mm thick) were placed above and below the powder bed, and a layer of graphoil (0.26 mm thick) and boron nitride spray between the molybdenum sheets and the graphite spacers. This assembly prevented the alumina samples from bonding to the graphite spacers, and reduced carbon contamination from the graphite die. 6.0 grams of the sieved powder were poured into the graphite die, and uniaxially cold-pressed at approximately 7 MPa to initially consolidate the powder (determination of the green density of the powder compacts at this stage is discussed below). The resistively heated graphite hot-press furnace (Centorr, Testorr™ series) was constructed such that it sits within a hydraulic load frame (MTS, Model 312.21). The assembled graphite die was placed in the furnace chamber and a vacuum was pumped for approximately 12 hours, until a 40-50 mTorr (5.3-6.7 Pa) vacuum was achieved, and a vacuum of better than 150 mTorr (20 Pa) was maintained from room temperature to 1550°C. At 1550°C, the vacuum was turned off and the furnace chamber was backfilled with high-purity gettered nitrogen, which continuously flowed at approximately 4 L/min and 2 psi (1.4×10^4 Pa) for the remainder of the hot-press run. A vacuum atmosphere was reported to be beneficial for removing volatiles during hot pressing of transparent ceramics.[28] However, alumina will severely react with graphite under a vacuum atmosphere above 1600°C,[33,42] whereas only minimal reactions were observed in a nitrogen atmosphere even up to 1825°C in this study. The preload pressure (P_i, 0-8 MPa) was applied to the die at room temperature and maintained during heating (25°C/min) to the maximum temperature. For $P_i = 0$ MPa, the top platen of the load frame was positioned ~5 mm away from the top ram of the assembled hot-press die, allowing the die to expand freely during heating. The furnace was controlled by a C-type thermocouple positioned near the edge of the graphite die for temperatures up to 1500°C, and a pyrometer viewing the edge of the graphite die for temperatures above 1500°C. When the furnace reached the maximum temperature (T_{max}, 1750-1825°C), the maximum pressure (P_{max}, 2.5-80 MPa) was applied at a rate of 1.3 MPa/min. After the maximum pressure was achieved, the furnace was held at T_{max} and P_{max} for the isothermal hold time (t_{iso}, 1-7 hours). The pressure was removed prior to cooling (25°C/min), and the ~2.8 mm thick transparent alumina sample was removed from the die. Load and ram displacement were recorded throughout the run.

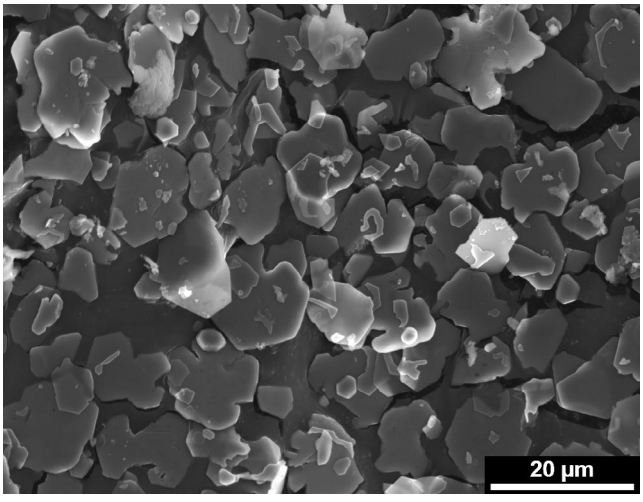

FIGURE 1 Scanning electron microscopy micrograph of ethanol-washed (P1) RonaFlair® platelet-morphology alumina powder

2.3 | Sample polishing, density measurements, microscopy, and X-ray diffraction

Hot-pressed samples were ground and polished to minimize surface scattering. A 100-grit metal-bonded diamond grinding wheel was used to machine equal amounts of material from each side of the samples to a thickness of approximately 1.5 mm. Both sides of the samples were polished down to a 1 μm diamond suspension, resulting in final thicknesses ranging from 1.15 to 1.40 mm.

The geometric green-body densities of the powder compacts at the start of a given hot-press run were determined. The mass of powder (6.0 g) and diameter of the compacts (25.4 mm) are constants, but the height of the compact will change depending on the powder type (EtOH-wash vs heat-treated) and preload pressure (0-8 MPa), resulting in different green-body densities. The heights of the compacts were determined by subtracting the height of an empty (no powder) hot-press die under a given preload pressure from the height of a prepared (6.0 g of powder) hot-press die under the same preload pressure. Geometric green-densities can then be calculated with this height, and are shown in Table 1. The densities of the hot-pressed samples were measured using the

TABLE 1 Processing parameters and microstructural properties of hot-pressed alumina samples

		Hot-Pressing Parameters				Relative Density (%TD)		
Sample ID	Powder and treatment	Max Temperature, T_{max} (°C)	Preload Pressure, P_i (MPa)	Max Pressure, P_{max} (MPa)	Isothermal Hold Time, t_{iso} (hr)	Green-body (geometric, ±0.1%)	Hot-pressed (Archimedes, ±0.03%)	Grain size (μm)
P1-1750-2-40-5	P1	**1750**	2	40	5	45.1	99.74	34.1±3.3
P1-1775-2-40-5	P1	**1775**	2	40	5	45.1	99.74	38.6±5.0
P1-1800-2-40-5	P1	**1800**	2	40	5	45.1	99.82	52.3±6.3
P1-1825-2-40-5	P1	**1825**	2	40	5	45.1	99.80	75.7±15.3
P2-1800-0-40-5	P2	1800	**0**	40	5	37.2	99.81	61.1±8.6
P2-1800-2-40-5	P2	1800	**2**	40	5	40.2	99.64	57.2±8.4
P2-1800-4-40-5	P2	1800	**4**	40	5	41.2	99.80	49.9±6.1
P2-1800-8-40-5	P2	1800	**8**	40	5	43.3	99.89	45.4±6.5
P2-1800-0-2.5-5	P2	1800	0	**2.5**	5	37.2	99.09	69.8±15.0
P2-1800-0-5-5	P2	1800	0	**5**	5	37.2	99.66	57.7±11.7
P2-1800-0-10-5	P2	1800	0	**10**	5	37.2	99.93	61.8±11.6
P2-1800-0-20-5	P2	1800	0	**20**	5	37.2	99.81	57.2±7.2
P2-1800-0-40-5	P2	1800	0	**40**	5	37.2	99.81	61.1±8.6
P2-1800-0-80-5	P2	1800	0	**80**	5	37.2	99.79	60.2±10.8
P2-1800-0-10-1	P2	1800	0	10	**1**	37.2	99.68	29.3±2.1
P2-1800-0-10-3	P2	1800	0	10	**3**	37.2	99.72	43.4±5.6
P2-1800-0-10-5	P2	1800	0	10	**5**	37.2	99.93	61.8±11.6
P2-1800-0-10-7	P2	1800	0	10	**7**	37.2	99.89	64.7±9.3
E3-1825-0-40-5[a]	E3	1825	0	40	5	N/A	99.96	92.0±20.3

The significance of the bold in the table is to highlight different sets of samples.

Powder P: Platelet morphology alumina powder, RonaFlair® White Sapphire, Merck KGaH.

Powder E: Equiaxed morphology alumina powder, AA03, Sumitomo.

Treatment 1: Ethanol-washed.

Treatment 2: Ethanol-washed & heat-treated at 1100°C for 1hr in air.

Treatment 3: As Received.

[a]Sample replicated with similar powder and parameters as Sellers et al.[39]

Archimedes method,[43] accounting for the temperature-density dependency of the distilled water (21.2°C), resulting in a standard error of ±0.09%. A commercially available piece of single-crystal sapphire was measured alongside the hot-pressed samples, resulting in a density of 3.977 g/cm^3. Relative densities of the samples were calculated by dividing their density by the density of the single-crystal sapphire standard, and are listed in Table 1.

Cross sections of the samples were polished to a 1μm diamond finish, and thermally etched at 1600°C for 30 minutes in air. The samples were sputter-coated with Au-Pd, and the microstructures were observed by scanning electron microscopy with a FEI Quanta650 at 10 kV. Line intercept analysis was performed, obtaining at least 200 intersections. The average intercept length was multiplied by the geometric factor 1.56 to obtain the average grain size.

The crystallographic orientation of the hot-pressed samples were determined via X-ray diffraction (XRD) on a Panalytical Empyrean Diffractometer (Malvern Panalytical Ltd). The instrument was equipped with a bent Ge incident beam monochromator that is tuned to transmit Cu $K\alpha_1$ radiation. Intensity was measured from a 2θ of 20°-95°. Scans of the top surfaces of the samples were obtained, and maximum intensities were normalized to a value of 1 for ease of comparison.

2.4 | Optical measurements

Optical measurements were made using a PerkinElmer Lambda 950 UV-VIS-NIR spectrophotometer equipped with an integrating sphere. The visible spectrum was measured from 200-800 nm using a photomultiplier tube detector, and the near-infrared (IR) spectrum was measured from 1000-2500 nm using a lead sulfide (PbS) detector. A wavelength of 645 nm was chosen as the representative value for optical

properties in this study, which is a similar wavelength used in the literature.[8,12,14] Total transmission, in-line transmission, reflection, and absorption can be measured using the spectrophotometer, and the forward and backward scattering can be derived from them.

Total transmission (T_T) was measured by placing the sample directly against the edge of the integrating sphere, allowing all light that passes through the sample to enter the integrating sphere and be measured. In-line transmission (T_{ILT}) was measured by positioning the sample approximately 60 cm away from a 1.0 cm diameter aperture placed in front of the integrating sphere. Given the distance between the sample and the aperture, as well as the diameter of the aperture, all light that is scattered at an angle greater than an approximately 0.5° cone is not measured. This falls under the definition of "Real In-Line Transmission," as defined by Apetz et al.[8] Reflection (R) was measured using an arrangement similar to that of Apetz et al,[8] where the sample was placed directly against an inlet on the back-side of the integrating sphere. Absorption (A) was measured using a configuration similar to the reflection measurement, except a diffuse reflective cover was placed behind the sample. A more detailed description of the absorption measurement and configuration is given in the Appendix.

Absorption, forward scattering (T_{FS}), and backward scattering (R_{BS}) are calculated by Equations (1)-(3), respectively:

$$A = \frac{I - I_{raw}}{2}, \tag{1}$$

$$T_{FS} = T_T - T_{ILT}, \tag{2}$$

$$R_{BS} = R - R_S, \tag{3}$$

where I is the incident beam, I_{raw} is the raw light intensity measured by the detector during the absorption measurement, and R_S is the surface reflection of a single-crystal sapphire sample that was ground/polished using the same procedures as the hot-pressed samples. The optical properties of the sapphire sample were measured and used as a comparison.

Total transmission, in-line transmission, forward scattering, backward scattering, and absorption of transparent polycrystalline ceramics are all thickness dependent.[3] A thicker sample will have a lower total and in-line transmission, and a higher forward scattering, backward scattering, and absorption. Grinding and polishing the hot-pressed samples to a consistent thickness was challenging, so it was necessary to normalize the optical properties of the samples to the same thickness. A modified version of Krell et al's equation[12] was used to normalize the optical properties of the hot-pressed samples to a thickness of 0.8 mm, which is the thickness most commonly reported in the literature.[5,8,12,14,18,19,21] A detailed description of these equations are given in the Appendix.

3 | RESULTS AND DISCUSSION

3.1 | Effect of maximum temperature

The maximum temperature (T_{max}) during hot pressing is important as there must be enough thermal activation to achieve adequate diffusion for densification. Figure 2 shows the ram displacement over time for samples hot-pressed at T_{max} between 1750°C and 1825°C. The displacement was normalized to zero at time equal to zero to show the total amount of displacement for each sample. To observe the sintering behavior during heating, a small preload pressure (P_i = 2 MPa) was applied. All curves initially increase due to thermal expansion, then begin to shrink at approximately 1175°C, indicating the onset of densification. An anomaly in the data is observed for all curves at ~1550°C, where the samples appear to suddenly expand then shrink. This expansion/shrinkage is due to the furnace chamber being backfilled with gettered nitrogen, which changes the pressure being exerted on the load cell. At T_{max} (1750-1825°C), the sudden shrinkage is due to the application of the maximum pressure. The onset of this shrinkage is offset by 1 minute for the different T_{max} because the respective temperature is reached after different times at a constant heating rate of 25°C/min. At the onset of pressure application, the rate of displacement is higher at higher maximum temperatures. This is because alumina will plastically deform more readily at higher temperatures.[37] After approximately 1.3 hours, the slope of each curve spontaneously decreases, which is discussed in more detail in a later section. Once the maximum pressure is reached after about 1.7 hours, continued shrinkage is minimal, as the powder bed has nearly completely densified.

It was found that an increase in T_{max} resulted in a minimal change in final sample densities and a significant increase in grain size, as shown in Table 1. Samples sintered at a T_{max} of 1750°C and 1825°C have a grain size of 34 and 75 μm, respectively. Heuer et al[22,37–39] used equiaxed alumina at T_{max} between 1810°C and 1880°C to fabricate transparent samples, resulting in grain sizes on the order of 50 μm. One such sample hot-pressed at T_{max} = 1880°C resulted in a grain size of 46 μm.[38] The larger grain size at lower temperatures observed in this study may be due to the larger starting particle size (11 μm diameter) of the platelet alumina powder, compared to the 0.3 μm diameter equiaxed alumina powder used by Heuer et al.[22,37–39]

The optical properties of samples hot-pressed at different T_{max} are shown in Figure 3. The total and in-line transmission both increase with increasing T_{max}. There are minimal losses due to backward scattering, which implies that these samples have very little porosity, as supported by the high relative densities of these samples (Table 1). Most of the optical losses are due to forward scattering and absorption, which decrease with increasing temperature. Accordingly, these samples still have

significant birefringence effects and impurities. A gray discoloration is observed in the bulk of all samples, and a severe black discoloration is observed at the outer perimeter of the sample hot-pressed at 1825°C (P1-1825-2-40-5). The reason for this is not clearly understood. However, 1825°C is close to the eutectic between alumina and aluminum-carbide,[44] so there may be some reaction occurring between the graphite die and the alumina powder. 1800°C was chosen as the optimal T_{max} to prevent such a reaction, but discoloration is still present in the interior of the hot-pressed samples. Therefore, parameters that have been reported to minimize this discoloration were explored.

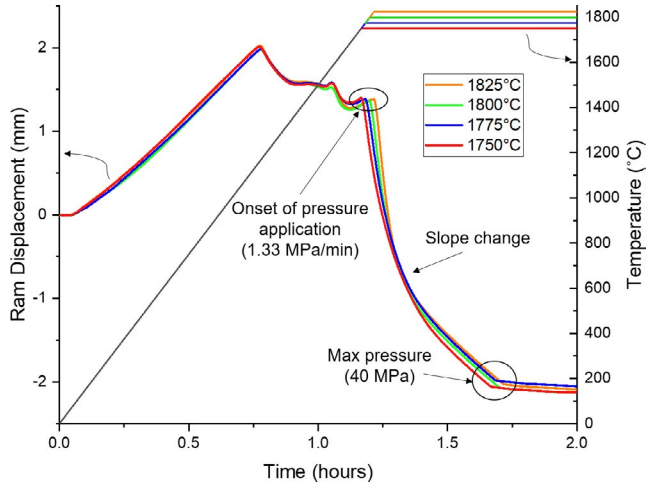

FIGURE 2 Ram displacement vs time of samples hot-pressed at different maximum temperatures

3.2 | Effect of powder heat treatment and preload pressure

The discoloration observed in the hot-pressed alumina samples is a defect that is common in transparent spinel.[40] Two methods were found in the literature that reduce this defect: a heat treatment of the powders prior to densification,[45] and an application of different preload pressures (P_i) during heating.[26,41] Both methods were explored in this study.

Figure 4 shows the ram displacement vs time for samples hot-pressed with or without a powder heat treatment, and at different preload pressures (P_i). Samples with $P_i = 2$, 4, and 8 MPa initially expand due to thermal expansion. No such expansion is observed for $P_i = 0$ MPa because the top platen of the load frame was not in contact with the assembled hot-press die, allowing the die to expand freely during heating. Samples hot-pressed at higher preload pressures expand at a slower rate, which is likely due to the higher preload pressures promoting particle rearrangement. Shrinkage begins at 1175°C for the ethanol-washed powders, and 1250°C for the heat-treated powders, indicating the onset of densification. This onset of densification at a lower temperature for the ethanol-washed powders may be due to it having a higher green-body density than the heat-treated sample: 45.1% (P1-1800-2-40-5) vs 40.2% (P2-1800-2-40-5), as shown in Table 1. However, when the onset of densification begins for the heat-treated powder samples, it occurs at a much faster rate than the ethanol-washed powder sample, and samples hot-pressed with higher P_i undergo more shrinkage (densification) during this stage due to the increased driving force for sintering from the applied P_i.[31] It is likely that by heat-treating the powder prior to densification, impurities in the powder are

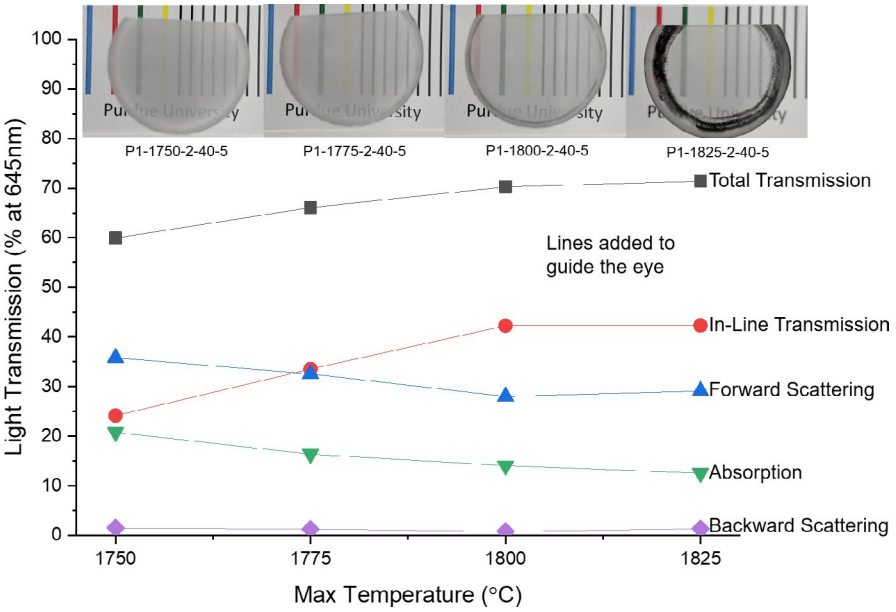

FIGURE 3 Light transmission as a function of maximum temperature, normalized to $t = 0.8$ mm. Samples are placed 2 cm above the text, in order of increasing temperature

removed,[40] which may allow the powder to densify more readily. High-temperature TGA of the different powder types showed that mass loss initiated around 825°C and 1200°C for the ethanol-washed powders and heat-treated powders, respectively. This confirms that some volatile species are being driven from the powders during the heat treatment. Chemical analysis of the powder indicates that sodium is the most prevalent impurity. The sodium is likely in the form of either sodium carbonate or sodium oxide, both of which thermally decompose well below the heat-treatment temperature of 1100°C.[46,47]

At the maximum temperature (T_{max} = 1800°C), the maximum pressure (P_{max} = 40 MPa) is slowly applied at a rate of 1.3 MPa/min. During this pressure-application step, the ethanol-washed powder (2 MPa, P1) experienced ~3.4 mm of shrinkage, while the heat-treated powder (2 MPa, P2) experienced ~3.8 mm of shrinkage. This difference in shrinkage is due to the ethanol-washed powder having a higher green density at the start of the hot-press run, as shown in Table 1. Additionally, the shrinkage during this step increases with decreasing preload pressure: ~1.7 mm at P_i = 8 MPa and ~6.6 mm at P_i = 0 MPa. This is because the green densities at the start of the hot-press run are lower at lower preload pressures (Table 1), yielding a greater amount of displacement when the maximum pressure is applied. For all samples, the slope of the curves spontaneously decreases after approximately 1.3 hours, similar to the behavior observed in Figure 2, and is discussed in more detail in a later section.

The effects of the powder heat treatment on the optical properties are shown in Figure 5. The ethanol-washed sample at P_i = 2 MPa (open shapes, P1-1800-2-40-5) has inferior optical properties compared to the heat-treated sample at P_i = 2 MPa (closed shapes, P2-1800-2-40-5). Losses due to absorption decreases for the heat-treated sample, suggesting that heat-treating the powder at 1100°C in air prior to hot pressing causes impurities to be driven off. Morita et al[45] found that heat-treating spinel powder prior to SPS improved the in-line transmission by 10%, which they claim to be due to impurities being reduced during the heat treatment. In this study, the heat treatment increased the in-line transmission of the hot-pressed platelet alumina by approximately 4%. As previously mentioned, high-temperature TGA indicates that some volatile species are being driven from the powders during the heat treatment, and sodium is likely the primary impurity being driven off. The removal of the sodium impurity from the powder prior to hot pressing may explain the decrease in absorption losses for the heat-treated samples. Additionally, TGA showed that some mass loss is still occurring beyond 1100°C, suggesting that a higher heat-treatment temperature, or even longer heat-treatment time, may additionally purify the powders and further reduce optical losses due to absorption.

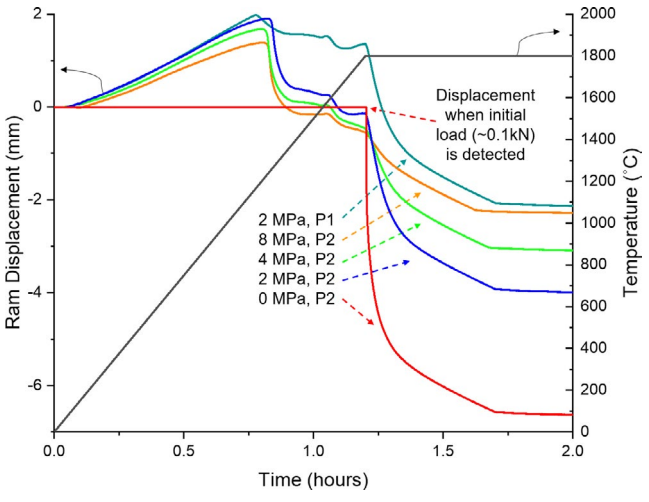

FIGURE 4 Ram displacement vs time of ethanol-washed (P1) and heat-treated (P2) samples hot-pressed at different preload pressures

Preload pressure has a more significant effect on the optical properties than heat treatment, as shown in Figure 5. The total and in-line transmission both decrease as P_i is increased. P_i has minimal effect on losses due to backward and forward scattering, suggesting that it has a minimal effect on the porosity. The similarities in the hot-pressed densities of these samples confirm this (Table 1). Losses due to absorption, however, notably increase with increasing P_i. Wang et al[26] observed a similar qualitative trend in spark plasma sintered spinel and attributed this to dislocations formed during densification. However, Merac et al[41] found that for hot-pressed spinel, it was beneficial to wait until higher temperatures before applying the maximum pressure, and they claimed that this allowed volatile species to escape from the unconstrained powder bed during heating. In this study, a similar phenomenon may be occurring, where a higher P_i results in a higher green-body density (Table 1), resulting in less open-porosity for volatiles species to escape. As a result, impurities are entrapped during fast sintering at high P_i, and thus more light lost due to absorption. Therefore, a lower P_i is preferred, with 0 MPa being optimal.

3.3 | Effect of maximum pressure

When hot-pressing ceramics, higher maximum pressure (P_{max}) generally results in higher densities and improved optical properties.[23,28] However, the slope-change of the ram displacement data in Figures 2 and 4 implies that there may be an optimum at lower pressures. To investigate this, samples hot-pressed at P_{max} of 2.5-80 MPa were studied, and the shrinkage rate vs time for these samples are shown in Figure 6. The shrinkage rate was calculated by taking the derivative of the displacement data. For each sample, the shrinkage rate is

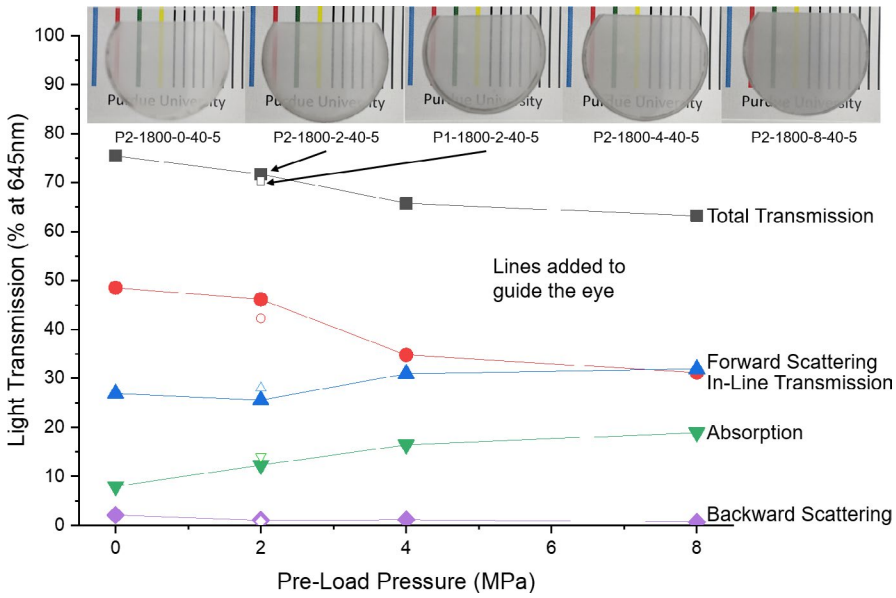

FIGURE 5 Light transmission as a function of preload pressure, normalized to 0.8 mm. Open points are samples with ethanol-washed powder (P1), and closed shapes are samples with heat-treated powder (P2). Samples are placed 2 cm above the text, in order of increasing pressure

initially high (>1 mm/min), and abruptly decreases when the respective P_{max} is achieved. The 2.5 and 5 MPa samples continue to shrink at a significant rate for approximately 10 minutes after reaching their respective P_{max}. This could be due to particle rearrangement, as well as a considerable amount of porosity remaining in the powder bed after these low pressures are applied.[48] On the other hand, the shrinkage rate of samples hot-pressed at $P_{max} \geq 10$ MPa abruptly decreases to virtually 0 mm/min after reaching their P_{max}. This is likely due to minimal porosity remaining at this higher pressure.

Another important feature of Figure 6 is the transition to a constant shrinkage rate of approximately 0.05 mm/min, which begins after approximately 10-minutes. This is more clearly seen in the inset plot. It is important to note that the pressure for all samples in this study was applied at a constant rate of 1.3 MPa/min, so this transition must be indicative of some phenomenon occurring during the slow application of maximum pressure. This transition corresponds to a pressure of approximately 15 MPa, so it occurs for samples with P_{max} of 20, 40, and 80 MPa. These samples go through this transition and maintain the constant shrinkage rate until their respective P_{max} is achieved, at which point the shrinkage rate promptly decreases to virtually 0 mm/min. It is thought that at pressures beyond 15 MPa, the powder bed has nearly completely densified, remaining porosity is closed-porosity, and any further pressure results in

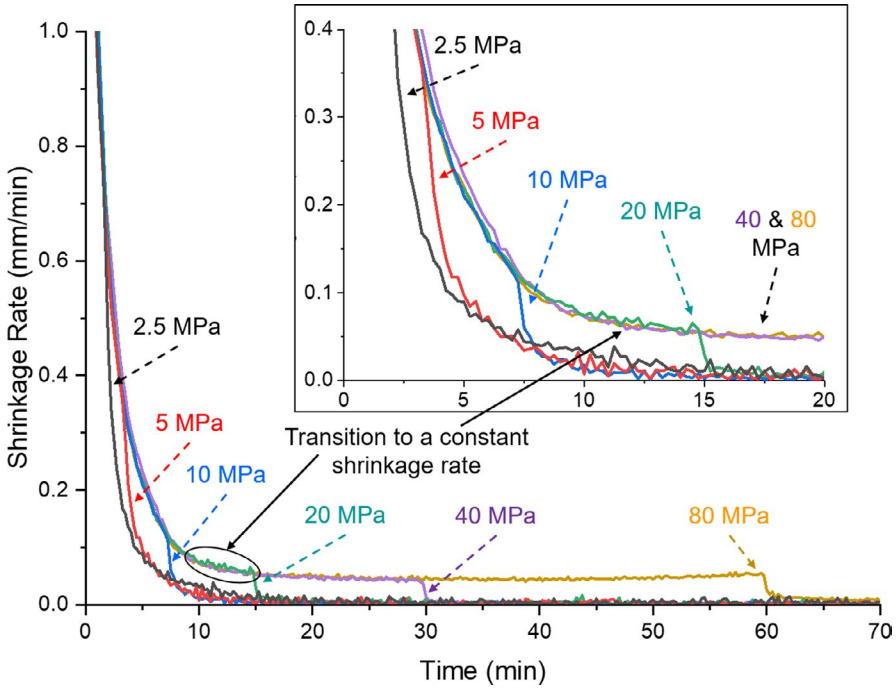

FIGURE 6 Shrinkage rate as a function of time for samples hot-pressed at different maximum pressures. The sudden decrease in each curve indicates when the maximum pressure was achieved

linear-elastic strain of the powder compact and graphite die assembly. Hot pressing at pressures beyond this transition results in a decrease in density, as shown in Table 1. Such results are contradictory to the commonly observed trend that higher pressures result in higher densities[23,28] (due to an increased driving force for sintering[48]). Therefore, hot pressing at a pressure that corresponds to the transition to a constant shrinkage rate appears to be optimal for this powder under these conditions. Heuer et al[22,37–39] used pressures between 27.5 and 46.8 MPa to achieve transparent alumina parts, but no discussion is given regarding the optimal pressure. They do, however, suggest that the hot-pressed parts must undergo a "critical strain" for recrystallization to occur.[22,37] Their initial experiments determined that a "critical strain" of more than 3.8% is necessary to induce primary recrystallization.[22] It is possible that the transition to a constant shrinkage rate of the current samples correspond to this "critical strain," though a more detailed analysis would be required to confirm this.

Table 1 shows the relative densities of samples hot-pressed at different maximum pressures. Relative density is low at lower maximum pressures (99.09% at $P_{max} = 2.5$ MPa), then increases with increasing maximum pressure (99.93% at $P_{max} = 10$ MPa). At maximum pressures beyond 10 MPa, the relative densities decrease with increasing maximum pressure (99.79% at $P_{max} = 80$ MPa), though differences in density at these pressures may not be statistically different. Lower pressures yielding lower densities is well understood: a lower pressure will result in less driving force for densification.[31] Higher pressures resulting in lower densities is not well understood. A possible explanation for this could be a pore-swelling phenomenon that occurs after the maximum pressure is removed. This can be shown by considering the internal pore pressure (P_p) during hot pressing:

$$P_p = P_{max} + \frac{2\gamma}{r_p}, \quad (4)$$

where P_{max} is the externally applied maximum pressure, γ is the surface energy of the pore-matrix interface, and r_p is the pore radius. Equation (4) shows that an increase in P_{max} will result in an increase in P_p. Additionally, r_p will decrease as the sample densifies, further increasing P_p, though the effect of decreasing pore size is minimal when compared to the externally applied maximum pressure. For example, at an externally applied pressure of 80 MPa, and if it is assumed that $\gamma = 1$ J/m^2 and $r_p = 0.5$ μm, the internal pore pressure will be 84 MPa. This means that the pore pressure will be effectively equal to the maximum pressure. As described in Section 2, the maximum pressure is released at the end of the isothermal hold, prior to cooling. It is thought that when P_{max} is released prior to cooling, P_p is still very high, and the surrounding matrix (which is still at temperatures >1700°C for several minutes) will creep to relieve the high pore pressure. The pores will swell, resulting in a lower density, and diminished optical properties. This effect will be exacerbated at higher P_{max} due to P_p scaling with P_{max}. Furthermore, the transition to a constant shrinkage rate (Figure 6) may correspond to the P_{max} at which the P_p is too high, resulting in pore swelling when the pressure is released.

It may be possible to mitigate this pore swelling phenomenon by maintaining P_{max} during cooling since the surrounding matrix cannot creep at lower temperatures. Literature regarding SPS of alumina reports that the pressure is typically maintained during cooling. Kim et al[17,19,20] spark plasma sintered alumina to transparency at 1150°C and 80 MPa for 20 minutes, followed by maintaining the 80 MPa of pressure during cooling to 1000°C. The authors note that this was done to relieve residual stresses.[17,19,20] However, maintaining the pressure until the system is cooled to 1000°C may have retained a smaller pore size since 1000°C may be low enough temperature to prevent the surrounding matrix to creep under the gas pressure and swell to a lower density.

The optical properties of samples hot-pressed at different P_{max} are shown in Figure 7. The total and in-line transmission both initially increase to a maximum at 10 MPa, then decrease with increasing P_{max}. Forward scattering, backward scattering, and absorption follow a reverse trend, where they initially decrease to a minimum at 10 MPa, then increase with increasing P_{max}. Forward scattering is the dominating mechanism of loss at all P_{max}. A considerable amount of light is also being lost due to absorption, and it reaches a minimum at 10 MPa, but this change in absorption is minimal compared to the changes observed in the other hot-pressing parameters. Backward scattering is also affected by differences in maximum pressure. Backward scattering is approximately 4% at 2.5 MPa, decreases to a minimum of 0.7% at 10 MPa, then increases with increasing P_{max} to 8.3% at 80 MPa. As mentioned earlier, backward scattering is due to residual porosity,[8] so it follows that both too low and too high of maximum pressure is resulting in some amount of porosity. The densities of these samples confirm this, as shown in Table 1, though the differences in densities for samples hot-pressed at $P_{max} > 10$ MPa may not be statistically significant.

It is notable that the best optical properties at 10 MPa corresponds with the transition to a constant shrinkage rate that was previously discussed. This further reinforces that the transition corresponds to a pressure that is high enough to ensure adequate pore removal yet is low enough to prevent the proposed pore swelling phenomenon. Adequate pore removal, as well as mitigated pore swelling, decreases backward scattering and improves the in-line transmission. Therefore, it was determined that 10 MPa is the optimal P_{max} for hot pressing this platelet alumina to transparency.

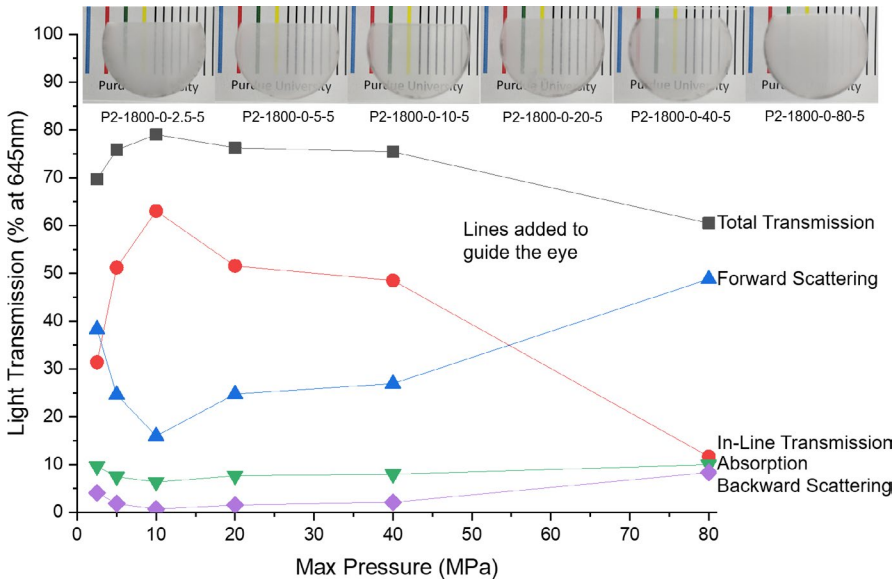

FIGURE 7 Light transmission as a function of maximum pressure, normalized to $t = 0.8$ mm. Samples are placed 2 cm above the text, in order of increasing pressure

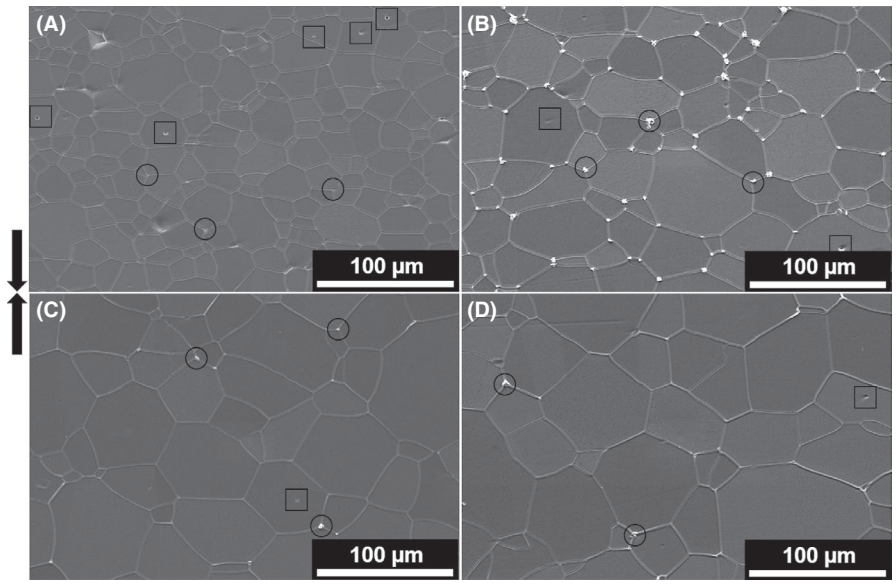

FIGURE 8 Scanning electron microscopy micrographs of samples hot-pressed for 1 (A), 3 (B), 5 (C), and 7 (D) hours. Circles and squares indicate inter and intra-granular porosity, respectively. The arrows indicate the hot-pressing direction

3.4 | Effect of isothermal hold time

To ensure adequate density after P_{max} is applied during hot pressing, an isothermal hold time (t_{iso}) is required.[33] However, it is important to determine the minimum amount of t_{iso} required to reach adequate densities, as a shorter time will result in smaller grain sizes.[48] Heuer et al discussed how sinter-forged alumina samples must undergo a certain amount of t_{iso} after primary recrystallization to fully densify.[22,37–39] Their studies showed that at least 2 hours are required to achieve adequate densities for transparency. As shown in Table 1, the density of samples hot-pressed at different t_{iso} increases with increasing hold time, particularly between 3 and 5 hours, while the density increase from 1-3 and 5-7 hours may not be statistically significant. Figure 8 shows the microstructure of samples hot-pressed at t_{iso} ranging from 1 to 7 hours. After 1 hour, there is a noticeable amount of intragranular porosity (squares). After 3 hours, large white phases (circles) are seen at the triple junctions. This could be the result of remaining secondary phases (impurities) diffusing out along the grain boundaries during thermal etching. After 5 hours, only a few intergranular pores remain, and after 7 hours, the sample is virtually pore-free. This densification at higher t_{iso} occurs at the expense of increased grain growth, as shown in Table 1 and Figure 8.

The optical properties of samples hot-pressed at different t_{iso} are shown in Figure 9. The total and in-line transmission both significantly increase with increasing t_{iso}. At least 5 hours are required to obtain best optical properties ($T_{ILT} > 60\%$). The in-line transmission increases from 1.6% at $t_{iso} = 1$ hour to 65.3% at $t_{iso} = 7$ hours. For all samples, forward scattering is the dominating mechanism of optical loss. Backward scattering

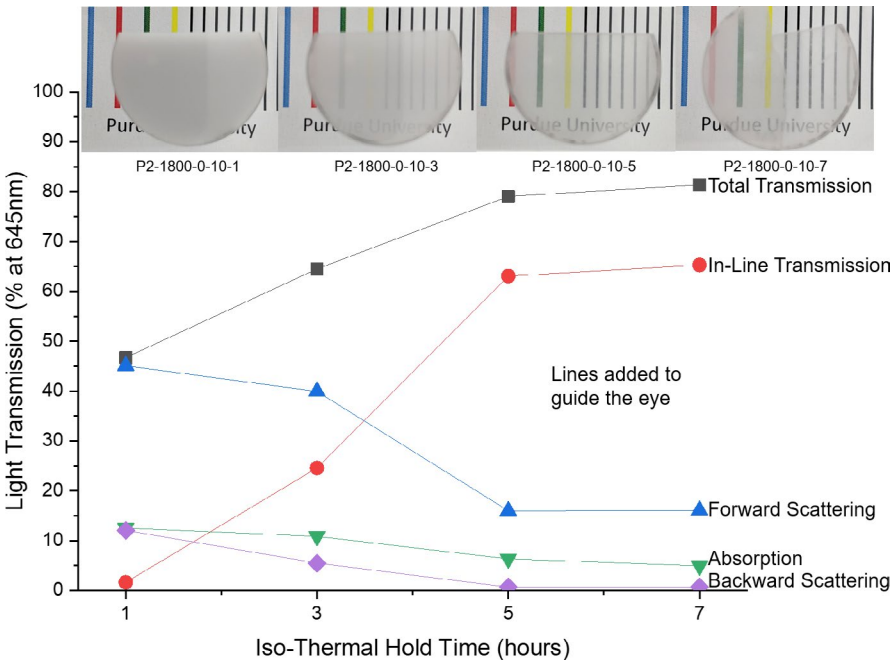

FIGURE 9 Light transmission as a function of isothermal hold time, normalized to $t = 0.8$ mm. Samples are placed 2 cm above the text, in order of increasing time

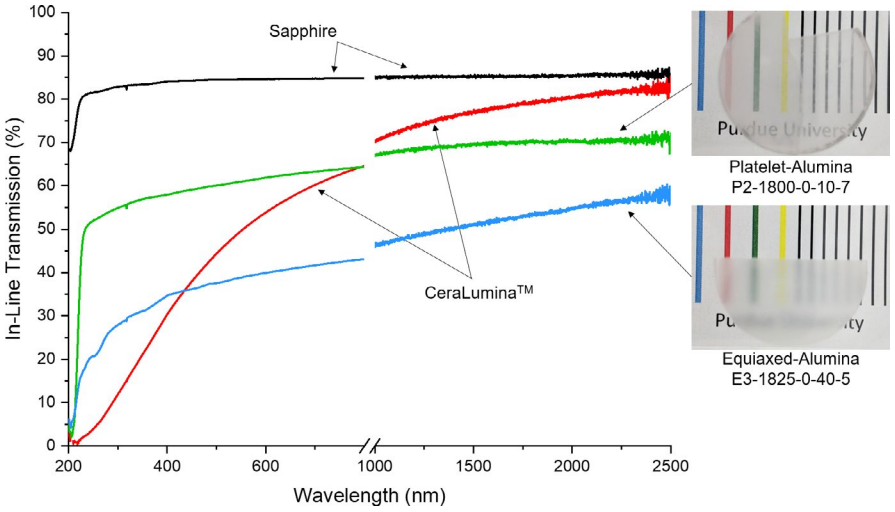

FIGURE 10 In-line transmission as a function of wavelength for a few comparative samples, normalized to $t = 0.8$ mm. Samples are placed 2 cm above the text

is significant at shorter t_{iso}, but decreases with increasing t_{iso}, indicating that the samples have lower porosity at longer t_{iso}. This is confirmed by the increasing density of the samples with increasing t_{iso}, as shown in Table 1. Absorption is also steadily decreasing with increasing t_{iso}. This is not well understood, though it is possible that residual impurities in the sample are driven off during longer t_{iso}. From this data it was concluded that increasing t_{iso} increases the final transparency.

3.5 | Comparison to transparent alumina using equiaxed morphology powders

Figure 10 shows the in-line transmission as a function of wavelength for the best platelet alumina sample produced in this study (P2-1800-0-10-7), a polished single-crystal sapphire standard, a commercially available transparent polycrystalline alumina sample (CeraNova's CeraLumina™), and a sample produced using equiaxed powder (E3-1825-0-40-5). The discontinuity between the visible and near-IR spectrums are due to the different detectors used. While the in-line transmission of the best platelet alumina sample does not reach the theoretical maximum of sapphire, it is markedly higher than the equiaxed-alumina, and is much higher than the commercially available sample in the visible spectrum. However, the in-line transmission of the commercially available sample surpasses the transmission of the best platelet alumina sample in the near-IR wavelength range. The reason for this is not currently understood, though it could be that grain size dependency begins to take prevalence at these higher wavelengths.

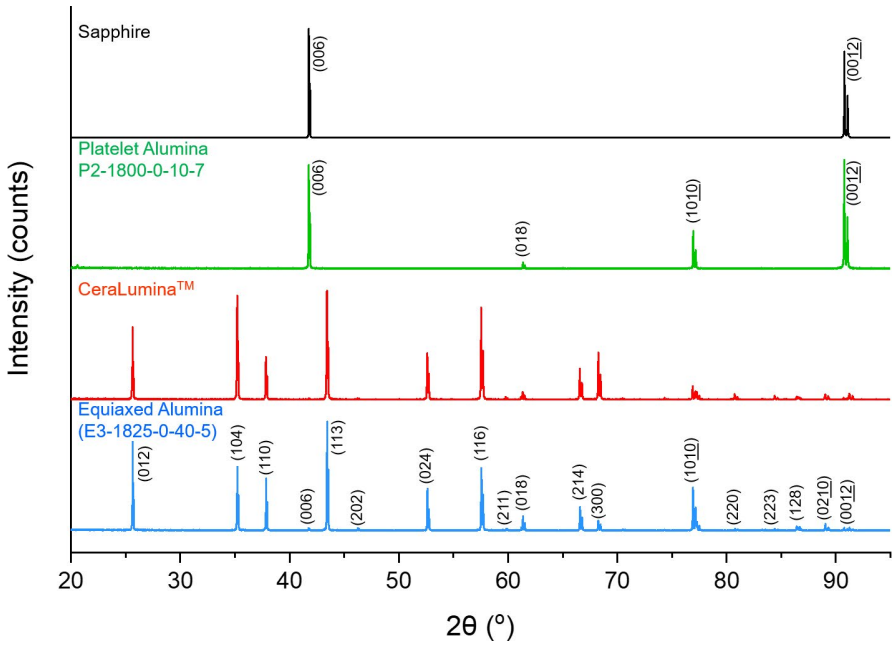

FIGURE 11 X-ray diffraction curves of a few representative samples, indicating differences in crystallographic orientation

The best platelet alumina sample in this study (P-1800-0-10-7) has an in-line transmission of 65.3% at 645 nm. At the time of publication, and to the best knowledge of the authors, this is the fourth highest in-line transmission reported for transparent alumina.[5,6,8,12,14] It is noteworthy that this platelet alumina sample was hot-pressed at lower pressures (10 MPa) when compared to equiaxed-alumina samples from HIP or SPS at higher pressures (>200 MPa).[8,12,14,21] This is particularly remarkable when the low intrinsic driving force for sintering of the large platelets (11 μm in diameter) is considered.

Another noteworthy observation is that the in-line transmission of the platelet alumina sample is high despite its large grain size (>60 μm; Table 1), as well as being relatively homogeneous across the entire optical spectrum (compared to the commercially available alumina sample) as shown in Figure 10. Both behaviors can be explained by Rayleigh-Gans-Debye theory,[8] which relates the in-line transmission of a birefringent polycrystalline ceramic to grain size (r), refractive index mismatch (Δn), sample thickness (d), and wavelength (λ_0), as shown in Equation (5):

$$T_{\mathrm{ILT}} = (1 - R_{\mathrm{S}}) \exp\left(-\frac{3\pi^2 r \Delta n^2 d}{\lambda_0^2}\right). \quad (5)$$

This theory shows that in-line transmission will increase with smaller grain sizes and lower refractive index mismatch, and will decrease at lower wavelengths.[8] However, refractive index mismatch has a much greater effect on the in-line transmission because it varies as Δn^2 (compared to r^1). Additionally, as Δn gets sufficiently low, it begins to negate wavelength dependence entirely. Because the platelet alumina sample has such a large grain size, the high and relatively homogeneous in-line transmission must mean that the refractive index mismatch is low. A low refractive index mismatch is related to high crystallographic orientation,[5,6,8] which implies that the samples in this study must have some degree of alignment.

X-ray diffraction curves of a few representative samples are shown in Figure 11. It is apparent that the (006) and (00$\underline{12}$) peaks, which are associated with the basal plane of sapphire, are very intense in the platelet alumina sample, while all peaks associated with the other crystallographic directions of alumina are nearly absent. Yi et al[6] observed similar trends in transparent alumina produced using a magnetic field to align equiaxed alumina prior to densification. They found that samples produced using a higher magnetic field resulted in higher in-line transmission, and XRD curves indicated that these samples had a high degree of crystallographic orientation. The crystallographic orientation in the present platelet alumina samples explains the high in-line transmission despite the large grain size. The crystallographic orientation minimizes birefringent scattering at the grain boundaries and reduces forward scattering losses. While the platelet alumina was not intentionally aligned prior to hot pressing, it is reasonable to assume that a majority of the high aspect-ratio platelets will tend to lie flat when poured into the die and compacted by uniaxial pressure. Additionally, Heuer et al[37] observed crystallographic orientation of their sinter-forged equiaxed alumina, so the present samples could be undergoing similar crystallographic orientation as a result of the hot-pressing parameters. The XRD curves of the equiaxed and CeraLumina™ samples are also shown in Figure 11, and the presence of peaks associated with all crystallographic directions indicates a lack of orientation, confirming that these samples have lower in-line transmissions due to birefringent scattering. Finally, while these 2θ XRD curves sufficiently indicate crystallographic orientation, they only provide a semiquantitative analysis of the amount of orientation and does not include any information about the exact

degree of mis-alignment of the grains.[49,50] A more effective analysis method, such as rocking curves or electron backscatter detection, will be used in future studies to study alignment of hot-pressed platelet alumina.

4 | SUMMARY AND CONCLUSIONS

The effect of hot-pressing parameters on the densification and optical properties of platelet-morphology alumina was analyzed. Increasing the maximum temperature improves the optical properties, at the expense of increased grain growth. However, the samples have a distinct gray discoloration. Heat-treating the powder prior to hot pressing and decreasing the preload pressure reduces the discoloration of hot-pressed samples, and hence reduces optical losses due to absorption. The heat treatment likely removes impurities, and a lower preload pressure may allow residual volatiles to escape the powder bed during hot pressing. A maximum pressure of 10 MPa yielded the highest in-line transmission. Pressures lower and higher than 10 MPa resulted in lower densities, which was confirmed by forward and backward scattering losses. Higher pressures resulting in lower densities is contrary to what is commonly observed in the literature and could be attributed to pore-swelling. It was found that >5 hours of isothermal hold time are required to achieve sufficiently high densities as required for transparency; however, this led to an increase in grain growth. Optical losses at short isothermal holding times are mainly due to backward scattering, which is indicative of residual porosity. A sample fabricated by hot-pressing heat-treated platelet alumina powder with a preload pressure of 0 MPa, a maximum temperature of 1800°C, a maximum pressure of 10 MPa, and an isothermal hold time of 7 hours yielded an in-line transmission of 65.3% at 645 nm, despite a large grain size of 65 μm. The high and relatively homogeneous in-line transmission despite the large grain size is explained by decreased refractive index mismatch at the grain boundaries due to crystallographic orientation.

ACKNOWLEDGMENTS

This study was financially supported by the Army Research Office (grant #W911NF-17-1-0203). The authors thank Dr Michael Bakas from the Army Research Office, Monica Viers, and Adam Smith for their assistance with processing, as well as Prof. John Blendell and Prof. Arthur Heuer for their fruitful discussions, and Merck KGaA (EMD Performance Materials) for providing the RonaFlair® platelet alumina powder.

ORCID

Andrew P. Schlup https://orcid.org/0000-0001-8403-0490
William J. Costakis https://orcid.org/0000-0002-0364-7227
Wolfgang Rheinheimer https://orcid.org/0000-0002-2906-4265
Rodney W. Trice https://orcid.org/0000-0002-8685-0289
Jeffrey P. Youngblood https://orcid.org/0000-0002-8720-8642

REFERENCES

1. Harris DC, Johnson LF, Cambrea L, Baldwin L, Baronowski M, Zelmon DE, et al. Refractive index of infrared-transparent polycrystalline alumina. Opt Eng. 2017;56(7):077103.
2. Krell A, Klimke J, Hutzler T. Advanced spinel and sub-μm Al_2O_3 for transparent armour applications. J Eur Ceram Soc. 2009;29(2):275–81.
3. Krell A, Klimke J, Hutzler T. Transparent compact ceramics: inherent physical issues. Opt Mater (Amst). 2009;31(8):1144–50.
4. Peelen JGJ. Transparent hot-pressed alumina, II: transparent versus translucent alumina. Ceram Int. 1979;5(3):115–9.
5. Mao X, Wang S, Shimai S, Guo J. Transparent polycrystalline alumina ceramics with orientated optical axes. J Am Ceram Soc. 2008;91(10):3431–3.
6. Yi H, Mao X, Zhou G, Chen S, Zou X, Wang S, et al. Crystal plane evolution of grain oriented alumina ceramics with high transparency. Ceram Int. 2012;38(7):5557–61.
7. Trice RW, Halloran JW. Investigation of the physical and mechanical properties of hot-pressed boron nitride/oxide ceramic composites. J Am Ceram Soc. 1999;82(9):2563–5.
8. Apetz R, Van BMPB. Transparent alumina: a light-scattering model. J Am Ceram Soc. 2003;86(3):480–6.
9. Zhang X, Liang S, Zhang P, Zhao T, Bai YU, Bao C-G, et al. Fabrication of transparent alumina by rapid vacuum pressureless sintering technology. J Am Ceram Soc. 2012;95(7):2116–9.
10. Coble RL. United States patent: transparent alumina and method of preparation. Alexandria, VA: United States Patent Office; 3,026,210, 1962.
11. Krell A, Hutzler T, Klimke J. Physics and technology of transparent ceramic armor: sintered Al_2O_3 vs cubic materials. In: Nanomaterials technology for military vehicle structural applications. Meeting Proceedings RTO-MP-AVT-122, Paper 14. Neuilly-sur-Seine, France: RTO, 2005. p. 14-1–10.
12. Krell A, Blank P, Ma H, Hutzler T, Van Bruggen MPB, Apetz R. Transparent sintered corundum with high hardness and strength. Am Ceram Soc. 2003;86(1):12–8.
13. Liu P, Yi H, Zhou G, Zhang J, Wang S. HIP and pressureless sintering of transparent alumina shaped by magnetic field assisted slip casting. Opt Mater Express. 2015;5(2):441.
14. Pringuet A, Takahashi T, Baba S, Kamo Y, Kato Z, Uematsu K, et al. Fabrication of transparent grain-oriented polycrystalline alumina by colloidal processing. Am Ceram Soc. 2016;99(10):3217–9.
15. Jiang D, Hulbert DM, Anselmi-Tamburini U, Ng T, Land D, Mukherjee AK. Optically transparent polycrystalline Al_2O_3 produced by spark plasma sintering. J Am Ceram Soc. 2007;91(1):151–4.
16. Prakasam M, Michau D, Viraphong O, Largeteau A. Optimal sintering parameters for Al_2O_3 optoceramics with high transparency by spark plasma sintering. Adv Appl Ceram. 2016;115(6):333–41.
17. Kim BN, Hiraga K, Morita K, Yoshida H, Miyazaki T, Kagawa Y. Microstructure and optical properties of transparent alumina. Acta Mater. 2009;57(5):1319–26.
18. Ashikaga T, Kim BN, Kiyono H, Suzuki TS. Effect of crystallographic orientation on transparency of alumina prepared using magnetic alignment and SPS. J Eur Ceram Soc. 2018;38(7):2735–41.
19. Kim BN, Hiraga K, Morita K, Yoshida H. Effects of heating rate on microstructure and transparency of spark-plasma-sintered alumina. J Eur Ceram Soc. 2009;29(2):323–7.
20. Kim BN, Hiraga K, Morita K, Yoshida H. Spark plasma sintering of transparent alumina. Scr Mater. 2007;57:607–10.

21. Grasso S, Yoshida H, Porwal H, Sakka Y, Reece M. Highly transparent α-alumina obtained by low cost high pressure SPS. Ceram Int. 2013;39(3):3243–8.
22. Rhodes WH, Sellers DJ, Heuer AH, Vasilof T. Development and evaluation of transparent aluminum oxide. Lowell, MA, 1967.
23. Peelen JGJ. Transparent hot-pressed alumina. I: hot pressing of alumina. Ceramurg Int. 1979;5(2):70–5.
24. Fu P, Xu Y, Shi H, Zhang B, Ruan X, Lu W. The effect of annealing process on the optical and microwave dielectric properties of transparent $MgAl_2O_4$ceramics by spark plasma sintering. Opt Mater (Amst). 2014;36(7):1232–7.
25. Morita K, Kim BN, Yoshida H, Hiraga K, Sakka Y. Influence of spark plasma sintering (SPS) conditions on transmission of $MgAl_2O_4$ spinel. J Am Ceram Soc. 2014;98(2):378–85.
26. Wang C, Zhao Z. Transparent $MgAl_2O_4$ ceramic produced by spark plasma sintering. Scr Mater. 2009;61(2):193–6.
27. Vu MT. Densification and characterization of transparent polycrystalline spinel produced by spark plasma sintering. Rutgers, 2014.
28. Rubat du Merac M, Kleebe HJ, Müller MM, Reimanis IE. Fifty years of research and development coming to fruition; unraveling the complex interactions during processing of transparent magnesium aluminate ($MgAl_2O_4$) spinel. J Am Ceram Soc. 2013;96(11):3341–65.
29. Munir ZA, Anselmi-Tamburini U, Ohyanagi M. The effect of electric field and pressure on the synthesis and consolidation of materials: a review of the spark plasma sintering method. J Mater Sci. 2006;41(3):763–77.
30. Coble RL. Mechanisms of densification during hot-pressing. In: Kuczynski GC, Hooton NA, Gibbon CF, editors. Sintering and related phenomena. New York, NY: Gordon and Breach, 1965. p. 329–50.
31. Coble RL. Diffusion models for hot pressing with surface energy and pressure effects as driving forces. J Appl Phys. 1970;41(12):4798–807.
32. McClelland JD. Kinetics of hot-pressing. Canoga Park, CA: Atomics International; 1961.
33. McClelland JD, Zehms EH. End-point density of hot-pressed alumina. Am Ceram Soc. 1962;46(2):77–80.
34. Mangsen GE, Lambertson WA, Best B. Hot pressing of aluminium oxide. J Am Ceram Soc. 1960;43(2):55–9.
35. Rice RW. Fabrication and characterization of hot pressed Al_2O_3. Washington, DC: Naval Research Lab; 1970.
36. Oudemans GJ. Continuous hot pressing. Philips Tech Rev. 1968;2(2):45–54.
37. Heuer AH, Sellers DJ, Rhodes WH. Hot working of aluminum oxide. 1: primary recrystallization and texture. J Amer Ceram Soc. 1969;52:468–74.
38. Rhodes WH, Sellers DJ, Vasilos T. Hot-working of aluminum oxide: 11, optical properties. J Am Ceram Soc. 1974;58(1–2):31–4.
39. Sellers DJP, Rhodes WHL, Vasilos TW. United States patent: method of preparing transparent alumina. Alexandria, VA: United States Patent Office; 3,899,560, 1975.
40. Morita K, Kim BN, Yoshida H, Hiraga K, Sakka Y. Spectroscopic study of the discoloration of transparent $MgAl_2O_4$ spinel fabricated by spark-plasma-sintering (SPS) processing. Acta Mater. 2015;84:9–19.
41. Rubat du Merac M, Reimanis IE, Smith C, Kleebe HJ, Müller MM. Effect of impurities and LiF additive in hot-pressed transparent magnesium aluminate spinel. Int J Appl Ceram Technol. 2013;10:E33–48.
42. Halmann M, Steinfeld A, Epstein M, Vishnevetsky I. Vacuum carbothermic reduction of alumina. Miner Process Extr Metall Rev. 2014;35(2):126–35.
43. ASTM Standard C693, 1993 (2013). Standard test method for density of glass by buoyancy. J ASTM Int. 1993;2013:1–3.
44. Foster LM, Long G, Hunter MS. Reactions between aluminum oxide and carbon: the Al_2O_3-Al_4C_3 phase diagram. J Am Ceram Soc. 1956;39(1):1–11.
45. Morita K, Kim BN, Yoshida H, Hiraga K, Sakka Y. Influence of pre- and post-annealing on discoloration of $MgAl_2O_4$ spinel fabricated by spark-plasma-sintering (SPS). J Eur Ceram Soc. 2016;36(12):2961–8.
46. Siriwardane RV, Poston JA, Robinson C, Simonyi T. Effect of additives on decomposition of sodium carbonate: precombustion CO_2 capture sorbent regeneration. Energy Fuels. 2011;25(3):1284–93.
47. Wigmans T, van Doorn J, Moulijn JA. Temperature-programmed desorption study of Na_2CO_3-containing activated carbon. Fuel. 1983;62(2):190–5.
48. Rahaman MN. Ceramic processing and sintering. 2nd edn. New York, NY: Marcel Dekker; 2003.
49. Seabaugh MM, Vaudin MD, Cline JP, Messing GL. Comparison of texture analysis techniques for highly oriented α-Al_2O_3. J Am Ceram Soc. 2004.
50. Vaudin MD, Rupich MW, Jowett M, Riley GN, Bingert JF. A method for crystallographic texture investigations using standard X-ray equipment. J Mater Res. 1998;13(10):2910–9.

How to cite this article: Schlup AP, Costakis WJ Jr., Rheinheimer W, Trice RW, Youngblood JP. Hot-pressing platelet alumina to transparency. *J Am Ceram Soc*. 2020;103:2587–2601. https://doi.org/10.1111/jace.16932

APPENDIX

As mentioned in Section 2, absorption was directly measured in this study. This was done by placing the samples against an inlet positioned behind the integrating sphere and a diffuse reflective cover placed behind the sample, as shown in Figure 12. This configuration, along with a simple Newtonian ray-diagram analysis, allows for a direct measurement of absorption. The incident beam, I, enters the integrating sphere and hits the sample, and some amount of light is reflected at the surface, R_S. The incident beam minus the surface reflectance beam continues to transmit through the sample, and some amount of it is lost due to absorption, A_1. The beam reflects off the diffuse reflective cover and is transmitted back through the sample a second time, and some amount of it is lost due to absorption again, A_2. The raw light intensity, I_{raw}, includes the surface reflection and the light that passed through the sample (indicated by bold arrows in Figure 12), and is given by Equation (6):

$$I_{raw} = I - R_S - A_1 - A_2 + R_S. \quad (6)$$

The reflection value cancels out, and for the absorption $A_1 = A_2 = A$ holds. Solving for A gives Equation (1).

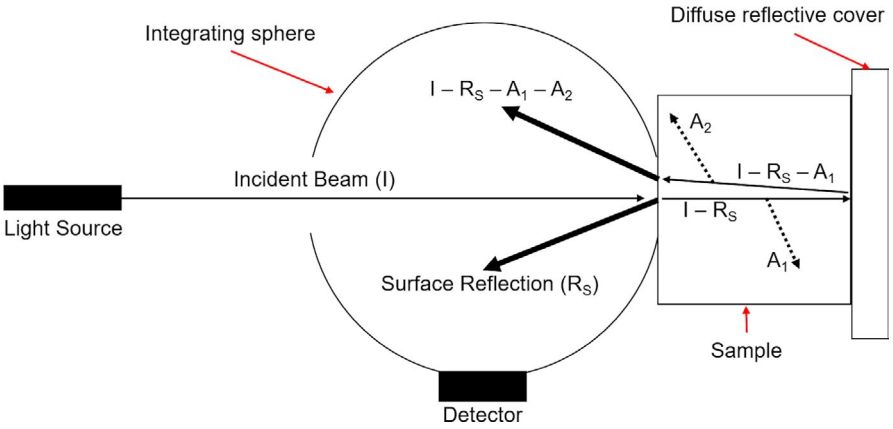

FIGURE 12 Ray diagram illustrating direct measurement of light absorption (modified from Apetz et al[8]). The bold arrows indicate the raw light intensity that is measured by the detector (I_{raw}), and the dotted lines indicate the light lost to absorption ($A_1 = A_2 = A$). This configuration and sample size are not to scale

A modified version of the equation by Krell et al[12] was used to normalize the optical properties of the hot-pressed samples to a thickness of 0.8 mm. Transmission was normalized via Equation (7):

$$T_n = (T_{SCS})\left(\frac{T_m}{T_{SCS}}\right)^{d_n/d_m}, \tag{7}$$

where T_n is normalized transmission, T_m is measured transmission, d_n is normalized thickness, d_m is measured thickness, and T_{SCS} is the transmission of the single-crystal sapphire standard. This equation was used to normalize both total and in-line transmission, and normalized forward scattering was then calculated using these normalized transmission values in Equation (2).

Reflection was normalized via Equation (8):

$$R_n = (R_S)\left(\frac{R_m}{R_S}\right)^{d_n/d_m}, \tag{8}$$

where R_n is normalized reflection, R_m is measured reflection, and R_S is the surface reflection of the polished single-crystal sapphire standard. Normalized backward scattering was then calculated using this normalized reflection in Equation (3).

The raw light intensity that is used to calculate absorption (Equation 1) was normalized via Equation (9):

$$I_{raw,n} = (I)\left(\frac{I_{raw,m}}{I_{SCS}}\right)^{d_n/d_m}, \tag{9}$$

where $I_{raw,n}$ is the normalized raw light intensity, $I_{raw,m}$ is the measured raw light intensity, and I_{SCS} is the raw light intensity of the single-crystal sapphire standard. Normalized absorption was then calculated via Equation (1).